Journal of
Synchrotron
Radiation

ISSN 1600-5775

Received 3 April 2014
Accepted 15 September 2014

Investigation of damaged interior walls using synchrotron-based XPS and XANES

Yingyot Poo-arporn,[a]* Surachai Thachepan[b] and Rungtiva Palangsuntikul[c]

[a]Synchrotron Light Research Institute, 111 University Avenue, Nakhon Ratchasima 30000, Thailand, [b]Department of Chemistry, Faculty of Science, Kasetsart University, 50 Phahonyothin Road, Bangkok 10903, Thailand, and [c]Biological Engineering Program, Faculty of Engineering, King Mongkut's University of Technology Thonburi, 126 Pracha Uthit Road, Bangkok 10140, Thailand. *E-mail: yingyot@slri.or.th

Evidence of internal sulfate attack in field exposure was demonstrated by the damaged interior wall of a three-year-old house situated in Nakhon Ratchasima Province, Thailand. Partial distension of the mortar was clearly observed together with an expansion of a black substance. Removal of the black substance revealed a dense black layer. This layer was only found in the vicinity of the damaged area, suggesting that this black material is possibly involved in the wall cracking. By employing synchrotron-based X-ray photoelectron spectroscopy (XPS) and X-ray absorption near-edge structure (XANES) techniques, the unknown sample was chemically identified. The S 2*p* and O 1*s* XPS results mutually indicated the existence of sulfate species in the materials collected from the damaged area. The XANES results indicated the presence of ferrous (II) sulfate, confirming sulfate-induced expansion and cracking. The sulfate attack in the present case appeared to physically affect the structure whereas the chemical integrity at the molecular level of the calcium silicate hydrate phase was retained since there was a lack of spectroscopic evidence for calcium sulfate. It was speculated that internal sulfate probably originated from the contaminated aggregates used during the construction. The current findings would be beneficial for understanding the sulfate-attack mechanism as well as for future prevention against sulfate attack during construction.

Keywords: cement mortar; internal sulfate attack; cement; XPS; XANES.

1. Introduction

Sulfate attack is one of the most important phenomena affecting the durability of cement mortars and concrete. It is generally categorized as external or internal sulfate attack, depending on the source of sulfate ions (Ouyang *et al.*, 1988). External sulfate attack typically involves penetration of sulfate ions from solutions such as sea water and ground water to the concrete. Sulfate chemically reacts with hydrated cement and, as a consequence, ettringite and gypsum are formed as primary products (Chen & Jiang, 2009; Santhanam *et al.*, 2002, 2003; Tian & Cohen, 2000). This causes volume expansion and extensive cracking leading to the loss in strength and disruption of the structure. It has been reported that thaumasite can also be formed as a reaction product of sulfate attack at low temperature and causes the degradation of the hydrated cement structure. On the other hand, the internal sulfate attack involves the incorporation of sulfur- and/or sulfate-containing materials during the preparation period. Pyrite (FeS_2), naturally found in the earth's crust, is known to be one of the sulfur-rich minerals. This mineral can be readily oxidized in the presence of oxygen and moisture to produce sulfuric acid and iron sulfates (Lowson, 1982). The products contained in the aggregate materials can cause expansion, affecting the concrete durability. The reaction extent is dependent on the original grain size of the sulfide (Casanova *et al.*, 1996, 1997). Shayan reported the deterioration of the concrete surface of a ten-year-old hospital floor slab due to the oxidation of pyrite in the pyritic aggregate. It was observed that a considerable amount of pyrite was found in the aggregate used in the concrete in the blistering area (Shayan, 1988).

2. Experimental

The samples for measurements were prepared in solid form. The unknown black substance was collected from the damaged interior cement mortar wall. The standard compounds FeS_2 (99.9%, Alfa Aesar), $FeSO_4.7H_2O$ (99.999%, Alfa Aesar), $Fe_2(SO_4)_3$ (99.999%, Alfa Aesar), $Ca(OH)_2$ ($\geq$96%, Sigma-Aldrich), $CaCO_3$ (99.999%, Aldrich), CaO (99.9%, Aldrich) and $CaSO_4$ (99.0%, Sigma-Aldrich) were

used without further purification. The hydrated cement was prepared by mixing the cement with deionized water at a water:cement ratio of 20:1. The mixture was kept at room temperature for 24 h. The hydrated cement was filtered and dried at 313 K and kept in the desiccator prior to the measurement.

X-ray photoelectron spectroscopy (XPS) experiments were carried out at BL3.2a of the SLRI using the CLAM2 energy analyzer. The beamline employs a varied-line-spacing plane grating to monochromatize synchrotron radiation. The excitation energy was 600 eV. The working pressure was controlled within 10^{-8} mbar at ambient temperature.

X-ray absorption near-edge structure (XANES) measurements were performed at the time-resolved XAS (Bonn-SUT-SLRI) beamline of the Synchrotron Light Research Institute, Thailand (Poo-arporn *et al.*, 2012). The beamline employs an energy-dispersive monochromator equipped with a Si(111) single crystal and position-sensitive detector to obtain the XANES spectra. The spectra were recorded at an integration time of 1000 ms with an average of ten readouts.

3. Results and discussion

The studied cement mortars were collected from the damaged wall of a house situated in Nakhon Ratchasima Province, Thailand (Fig. 1*a*). The damage was found on a structural brick wall, covered with painted cement mortar at around 36 months after the construction. Partial distension of the mortar was clearly observed together with an expansion of a black substance. Removal of the black substance revealed a dense black layer under the pale brown cement mortar (Fig. 1*b*). The typical size of the crack area was approximately 20 mm × 20 mm and 3 mm in depth. The black layer expanded gradually as clearly seen in Fig. 1(*c*), which was taken seven months after the previous removal of the black substance. Drilling a 6 mm hole through the black layer revealed that the thickness of the black layer was about 2 mm. It was interesting that the black layer was only found in the vicinity of the damaged area, suggesting that this black material is possibly involved in the wall cracking. Further investigation on chemical properties of the black substance would provide significant information for the mechanism of the damages.

The black substance was sampled from the damaged wall and characterized using XPS. This technique is usually employed to identify the type and oxidation state of an element in a material of interest. The principle of XPS is based on the photoelectric effect. The interaction between X-rays with sufficient energy and the atoms produces photoelectrons which travel with kinetic energy (KE) given by

$$\mathrm{KE} = h\upsilon - \mathrm{BE} - \varphi_s, \tag{1}$$

where $h\upsilon$ is the energy of the photon, BE is the binding energy of the electron and φ_s is the spectrometer work function. Using an excitation energy of 600 eV, the black substance gave three intense XPS peaks consistent with O 1*s*, C 1*s* and S 2*p* (Fig. 2*a*). Additionally, the Auger electron peaks corresponding to O *KLL* and C *KLL* appeared in the range 60–160 eV and 305–390 eV, respectively. The results indicated that the black substance was composed of O and S. The observed signals from C were attributed to the carbon reference added during the sample preparation. It should be noted that the subtraction of the C 1*s* signal was impossible due to technical limitation. Since the black substance was collected from the damaged cement mortar, the contribution from Ca and Si was probably expected. The photoelectron peaks corresponding to

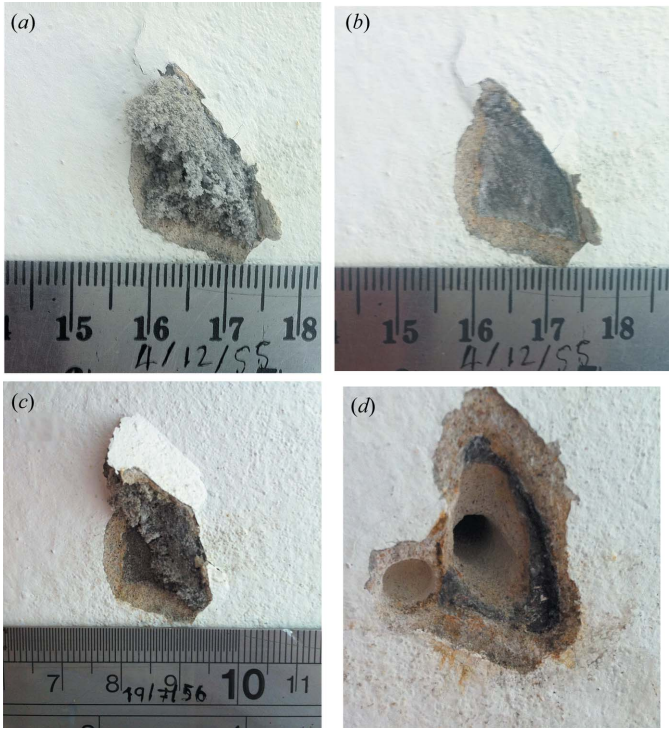

Figure 1
Photographs of the damaged area on the interior wall: (*a*) the crack was initially observed, (*b*) the same area after partial removal of the black substance, (*c*) seven months later, and (*d*) the same area after the expanded mortar.

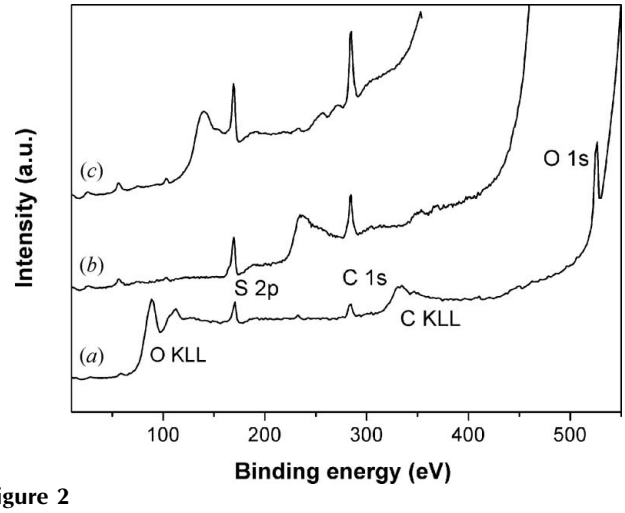

Figure 2
XPS spectra of the black substance collected from the cracked area. The survey scans were measured at a photon energy of (*a*) 600 eV, (*b*) 500 eV and (*c*) 400 eV.

Si 2*p* and Ca 2*p* were previously reported at 101 and 347 eV, respectively (Black *et al.*, 2003). It was clear that the photoelectron energy of Si 2*p* significantly overlapped the Auger electron peaks of O *KLL* and that of Ca 2*p* lay in the energy range of C *KLL*. To justify the contribution from Ca and Si, the photoelectron peaks were technically shifted from the Auger region by changing the excitation energy. The XPS spectra collected by tuning the excitation energy to 500 eV (Fig. 2*b*) and 400 eV (Fig. 2*c*) clearly showed no significant XPS peak corresponding to Ca 2*p* and Si 2*p*. Therefore, XPS results suggested that the black substance was a sulfur-rich compound.

The fine-scanned S 2*p* XPS spectra of the black substance with curve fitting showed only a single type of sulfur at the binding energy of 169.5 eV, consistent with sulfur of the sulfate (Fig. 3*a*) (Paneva *et al.*, 2007). The fine scan for O 1*s* displayed a broad and asymmetric feature due to contributions from different oxygen species (Fig. 3*b*). Peak fitting analysis demonstrated two binding energies at 530.9 and 532.0 eV, which could be ascribed to the oxygen bound to sulfur and hydroxyl group, respectively (Huang *et al.*, 2008). The binding energy of oxygen–sulfur significantly indicated the presence of sulfate in the black substance. The presence of hydroxyl groups in the cement mortar is predictable since $Ca(OH)_2$ is typically produced during the hydration of cement (Kirby & Biernacki, 2012).

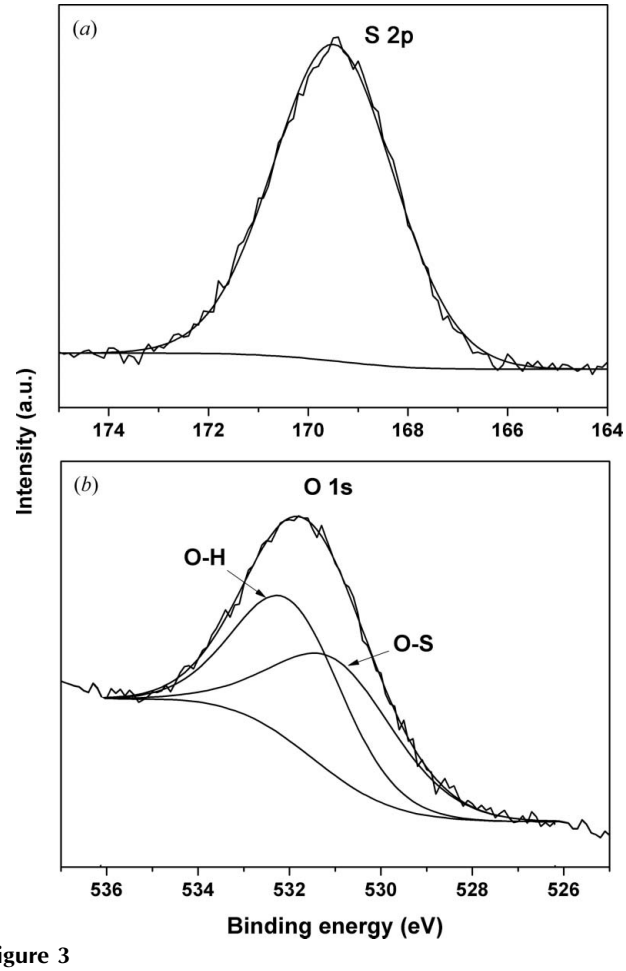

Figure 3
Fine-scan (*a*) S 2*p* and (*b*) O 1*s* XPS spectra of the black substance with the curve fitting.

The sulfur in the black substance potentially originated from the aggregates used during the construction. Generally, sulfur-containing compounds can be naturally found in both oxidized and reduced forms. Examples of the oxidized forms of sulfur are sulfoxide, sulfone, sulfonate and sulfate whereas the reduced forms include thiophene and sulfide (Prietzel *et al.*, 2007). Pyrite (FeS_2) is one of the most common sulfur-containing compounds found on the earth's crust. Mechanochemical treatment destabilized the pyrite and resulted in the formation of $Fe_2SO_4.H_2O$ (Godočíková *et al.*, 2002). In addition, the presence of oxygen and moisture could also oxidize the pyrite to produce ferrous sulfate through the reaction (Sammut *et al.*, 1996)

$$FeS_2 + \tfrac{7}{2}O_2 + H_2O \rightarrow Fe^{2+} + 2SO_4^{2-} + 2H^+. \qquad (2)$$

The oxidation of iron pyrite has been previously studied (Singer & Stumm, 1970). The oxygenation reaction of Fe^{2+} occurs in the presence of molecular oxygen. However, the half-time of the reaction in acidic pH is approximately 1000 days, which is relatively slow when compared with the oxidation of pyrite. The atmospheric oxidation reactivity of the surface of pyrite is dependent on species and abundance of such species on a freshly fractured surface (Chandra & Gerson, 2010). Further investigation by the XPS measurement of Fe was required to determine the involved iron species. However, it should be noted here that the signals of Fe 3*s* and 3*p* were very weak and that the measurement of Fe 2*p* XPS spectra was not reported due to the insufficient photon flux at excitation energy higher than 600 eV.

The other spectroscopic technique, *i.e.* XANES, was utilized in order to verify the involvement of iron in the black substance. XANES is an extremely useful characterization technique as it provides element-specific data as well as local-symmetry information as a consequence of multiple scatterings of the photoelectron (Bianconi, 1988). In this study, Fe *K*-edge XANES measurements of the unknown sample were carried out and compared with the spectra of the known standard compounds. Fig. 4 illustrates the normalized Fe *K*-edge XANES spectra of the black substance together with the standard FeS_2, $FeSO_4$ and $Fe_2(SO_4)_3$. Typical absorptions of the Fe *K*-edge were in the energy range 7125–7128 eV. The presence of the Fe *K*-edge XANES signal in the spectrum collected from the black substance clearly indicated the existence of iron in the sample. Significantly, the white line of Fe *K*-edge XANES together with the oscillation feature measured from the sample exactly resembled that of the standard $FeSO_4$, suggesting their chemical similarity. The contrast XANES results between the sample and either FeS_2 or $Fe_2(SO_4)_3$ ruled out the existence of both species in the black substance. One might also comment on the smaller intensity of the white line of the sample than that of the standard $FeSO_4$. In fact, the difference in intensity of the white line was generally observed (Lytle *et al.*, 1979; Sham, 1985). The energy of the white line of Fe *K*-edge XANES is due to the electronic transition from $1s \rightarrow p$ states. This absorption

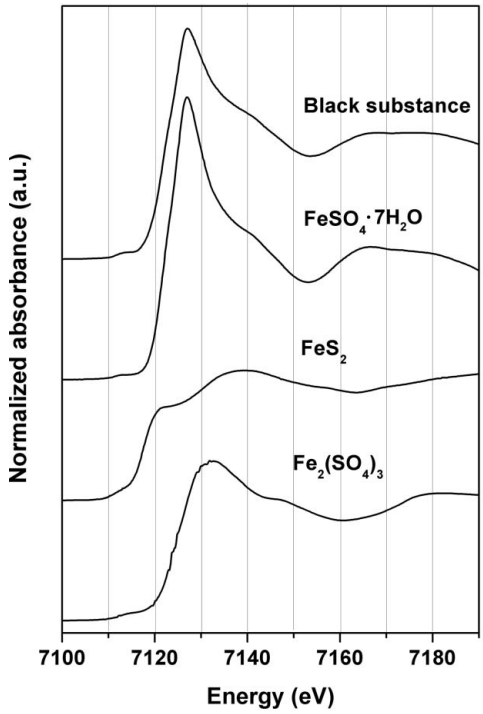

Figure 4
Fe *K*-edge XANES spectra of the black substance and the standard compounds.

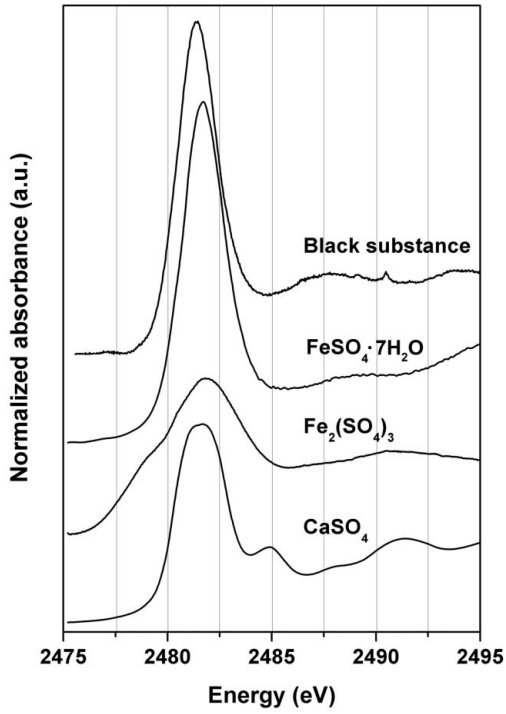

Figure 5
S *K*-edge XANES spectra of the black substance and the standard compounds.

cross section is strongly influenced by 3*p*–3*d* hybridization. In such a system where the *p*–*d* hybridization is weak, the *p*-like density of states is strongly reduced and only weak structures are observed in this region. Therefore, its intensity is proportional to the density of states of the unoccupied electronic level, related to the Pauling ionicity of the metal–ligand bonds of the compounds (Short *et al.*, 1983; Sinfelt *et al.*, 1981). In this case, the smaller white line peak of the sample suggested the smaller Pauling ionicity between Fe^{2+} and the sulfate ligand.

In order to confirm the above findings, the speciation of sulfate was further examined. The S *K*-edge XANES spectra of the compounds containing sulfur with oxidation state of +6 were measured (Fig. 5). Although the white-line energy of the S *K*-edge XANES of the black substance at 2481.5 eV was quite close to those of the standard $FeSO_4$, $Fe_2(SO_4)_3$ and $CaSO_4$ at 2481.6, 2481.8 and 2481.6 eV, respectively, the presence of $Fe_2(SO_4)_3$ and $CaSO_4$ was ruled out. The difference in the appearance of S *K*-edge XANES between these standard sulfate-containing compounds is due to the sensitivity on multiple scattering of the excited electron to multi-atom correlations. This electron confers sensitivity to the spatial arrangement of the neighbouring atom including radial distance, orientation and bond angle. In addition, a small shift of the white line between the black substance and standard $FeSO_4$ suggests the appearance of an alternate donating atom around S.

It is commonly known that the formation of gypsum ($CaSO_4.2H_2O$) occurs especially at the condition of high sulfate concentration. However, the appearance of the characteristic small post-edge peak at 2485 eV in the spectrum of $CaSO_4$ but not in that of the sample suggested that the presence of $CaSO_4$ in the sample was improbable. In addition, the spectrum of $Fe_2(SO_4)_3$ also showed different pre-edge and post-edge features compared with that of the sample, implying that the contribution from $Fe_2(SO_4)_3$ was irrelevant. Therefore, the above results implied that the black substance is comprised of iron and sulfur in the form of $FeSO_4$.

The effect of sulfate on the cement mortar was investigated in order to gain information and understand the mechanism of the sulfate attack. Typically, tricalcium silicate (C_3S) is the main phase of the clinker in Portland cement. The hydration products usually consisted of calcium silicate hydrate of variable stoichiometry, denoted as C-S-H (Kirby & Biernacki, 2012). The sulfate attack on the cement mortar usually produces a mineral phase containing calcium and sulfate, namely ettringite and gypsum. Fig. 6 shows the normalized Ca *K*-edge XANES spectra of the black substance and the standards, $Ca(OH)_2$, $CaCO_3$, CaO and $CaSO_4$. The fully hydrated cement was also used for comparison. The white-line peaks of the black substance, the hydrated cement, $Ca(OH)_2$, $CaCO_3$ and CaO were observed at 4044.7 eV, 4044.7 eV, 4045.7 eV, 4049.1 eV and 4051.0 eV, respectively. Clearly, the white-line peak of the C-S-H phase in the hydrated cement appeared at lower energy than that of the standard CaO, suggesting the formation of $CaO:SiO_2$ solid solution. In addition, $Ca(OH)_2$ commonly precipitates as portlandite during the cement hydration. Therefore, the Ca *K*-edge XANES of the hydrated cement was probably due to the contribution from both CaO and $Ca(OH)_2$. Significantly, the Ca *K*-edge XANES spectrum of the black substance was precisely identical to that of the hydrated cement, indicating the similarity of their local

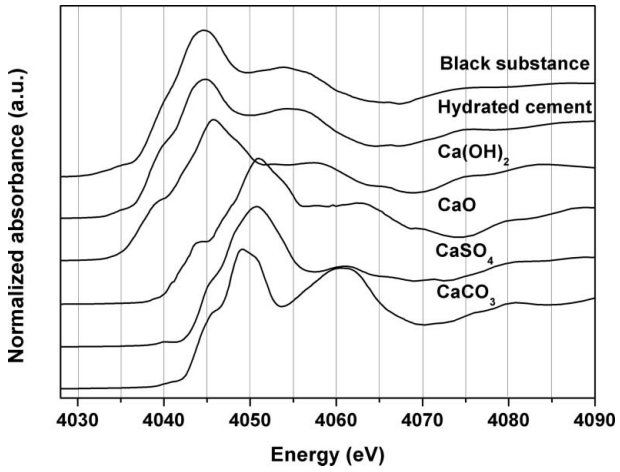

Figure 6
Ca *K*-edge XANES spectra of the black substance and the standard compounds.

structures. As the Ca *K*-edge XANES spectra of $CaCO_3$ and $CaSO_4$ were clearly distinguishable from that of the black substance, the presence of both compounds in the cement mortar was excluded. The overall results indicated that the local structure of the C-S-H phase in the cement mortar was insignificantly disturbed by the sulfate. Therefore, the observable expansions and cracks on the interior wall made of cement mortar were presumably the consequence of the precipitation of $FeSO_4$ phase rather than the attack of sulfate on the molecular structure of the C-S-H phase. It was noticed in this case that only the physical appearance of the interior wall was damaged but the chemical identity of the cement mortar remained unchanged.

4. Conclusions

Expansion and cracking of the cement mortar were shown from the damaged interior wall of a three-year-old house. By employing the powerful combination of X-ray photoelectron spectroscopy and X-ray absorption spectroscopy, identification of the oxidation state and local structure of the unknown compound was accomplished. In the present investigation the unknown black substance formed within the cracked cement mortar was mainly comprised of iron and sulfur in the form of the $FeSO_4$ phase as indicated by the S 2*p* and O 1*s* XPS results. Further investigation by the Fe *K*-edge and S *K*-edge XANES measurements confirmed the presence of the $FeSO_4$ structure. The precipitation of this phase within the mortar caused local expansion and cracking. The formation of the $FeSO_4$ phase appeared to affect only the physical strength of the mortar whereas the structure at the molecular level of the C-S-H phase was essentially unperturbed. The lack of evidence for the $CaSO_4$ phase implied that the chemical stability of the C-S-H phase against the sulfate attack as the extraction of calcium ions from the structure was impossible. The sulfate attack in this case is believed to occur internally as the interior wall was free from external sulfate species. It is speculated that the internal sulfate probably originated from the contaminated aggregates used during the construction. Further investigation on the chemical constituent of the aggregates would provide valuable information for the origin of the internal sulfate species.

The authors would like to thank P. Kinkhunthod, W. Saengsui and S. Chotowan for technical assistance on XANES measurements. Special thanks to H. Nakajima and S. Rattanasuporn for XPS data analysis. RP gratefully acknowledges financial support from the Thailand Research Fund (TRF) and the Office of the Higher Education Commission (grant number MRG5480179), the Higher Education Research Promotion and National Research University Project of Thailand, Office of the Higher Education Commission. ST acknowledges financial support from the Thailand Research Fund (MRG5380079), the Science Research Fund (ScRF-E7/2553 and E4/2554) from Faculty of Science, Kasetsart University and Kasetsart University Research and Development Institute (KURDI).

References

Bianconi, A. (1988). *X-ray Absorption: Principles, Applications, Techniques of EXAFS, SEXAFS and XANES*, edited by D. C. Koningsberger and R. Prins, pp. 573–662. New York: Wiley Interscience.
Black, L., Stumm, A., Garbev, K., Stemmermann, P., Hallam, K. R. & Allen, G. C. (2003). *Cem. Concr. Res.* **33**, 1561–1565.
Casanova, I., Aguado, A. & Agulló, L. (1997). *Cem. Concr. Res.* **27**, 1627–1632.
Casanova, I., Agulló, L. & Aguado, A. (1996). *Cem. Concr. Res.* **26**, 993–998.
Chandra, A. P. & Gerson, A. R. (2010). *Surf. Sci. Rep.* **65**, 293–315.
Chen, J. & Jiang, M. (2009). *Constr. Build. Mater.* **23**, 812–816.
Godočíková, E., Baláž, P., Bastl, Z. & Brabec, L. (2002). *Appl. Surf. Sci.* **200**, 36–47.
Huang, J., Wang, X., Hou, Y., Chen, X., Wu, L., Wang, X. & Fu, X. (2008). *Microporous Mesoporous Mater.* **110**, 543–552.
Kirby, D. M. & Biernacki, J. J. (2012). *Cem. Concr. Res.* **42**, 1147–1156.
Lowson, R. T. (1982). *Chem. Rev.* **82**, 461–497.
Lytle, F. W., Wei, P. S. P., Greegor, R. B., Via, G. H. & Sinfelt, J. H. (1979). *J. Chem. Phys.* **70**, 4849–4879.
Ouyang, C., Nanni, A. & Chang, W. F. (1988). *Cem. Concr. Res.* **18**, 699–709.
Paneva, D., Mitova, D., Manova, E., Kolev, H., Kune, B. & Mitov, I. (2007). *J. Min. Metall. B*, **43**, 57–70.
Poo-arporn, Y., Chirawatkul, P., Saengsui, W., Chotiwan, S., Kityakarn, S., Klinkhieo, S., Hormes, J. & Songsiriritthigul, P. (2012). *J. Synchrotron Rad.* **19**, 937–943.
Prietzel, J., Thieme, J., Salome, M. & Knicker, H. (2007). *Soil Biol. Biochem.* **39**, 877–890.
Sammut, J., White, I. & Melville, M. D. (1996). *Mar. Freshw. Res.* **47**, 669–684.
Santhanam, M., Cohen, M. D. & Olek, J. (2002). *Cem. Concr. Res.* **32**, 915–921.
Santhanam, M., Cohen, M. D. & Olek, J. (2003). *Cem. Concr. Res.* **33**, 341–346.
Sham, T. K. (1985). *Phys. Rev. B*, **31**, 1888–1902.
Shayan, A. (1988). *Cem. Concr. Res.* **18**, 723–730.
Short, D. R., Mansour, A. N., Cook, J. W. Jr, Sayers, D. E. & Katzer, J. R. (1983). *J. Catal.* **82**, 299–312.
Sinfelt, J. H., Via, G. H., Lytle, F. W. & Greegor, R. B. (1981). *J. Chem. Phys.* **75**, 5527–5537.
Singer, P. C. & Stumm, W. (1970). *Science*, **167**, 1121–1123.
Tian, B. & Cohen, M. D. (2000). *Cem. Concr. Res.* **30**, 117–123.